Lecture 3

The Sequence-of-Bifurcation Approach for the Transition to Turbulence

F. H. Busse

Notes by U. Riemenschneider and S. Plasting

1 Introduction

In this lecture we will discuss fluid systems in which there is a gradual evolution from the basic laminar state toward a turbulent state with increasing Reynolds number. Transition is seen to occur through a sequence of bifurcations. We consider fluid systems with a high degree of symmetries which in the laboratory are observed to undergo transition to complex flow states through supercritical bifurcations that are characterized by the breaking of flow symmetries. We will not consider systems such as pipe flow or plane Couette flow which exhibit strongly subcritical bifurcations from the basic laminar state to a turbulent state. Figure 1 shows some fluid systems with maximum symmetry which undergo gradual transtion from the basic state to ever more complex solutions. For each of these systems the external conditions are homogeneous in two spatial dimensions and in time and since we are dealing with systems far from thermodynamic equilibrium we must have inhomogeneity in the third spatial dimension along which a constant energy flux is applied, thus these systems exhibit maximum symmetry. Although these systems do not represent all important processes in fluid mechanics a large number of system can be idealized or reduced to their physically essential properties such that they conform to this high degree of symmetries.

The sequence-of-bifurcations approach discussed in this lecture has the following advantages

1. In most cases the reduction of inhomogeneity to a single dimension reduces a physical mechanism to its simplest form.

2. The homogeneity in two spatial dimensions and in time provides a maximum of symmetries, the breaking of which identifies the bifurcations in the manifold of solutions for the fluid flow.

3. The relative simplicity of the physical properties is reflected in the simplifications of the numerical analysis. Symmetries can be employed to reduce the numerical effort.

4. Although physically realized systems can only approximate homogeneity in two spatial dimensions, the bifurcations of the ideal system become only slightly imperfect bifurcations in the real system as long as the typical wavelengths introduced by bifurcating solutions are small in comparison to the length scales associated with the deviations from homogeneity.

5. The spatially and time periodic solutions that are obtained in the sequence-of-bifurcation approach represent only a minute manifold of the realizable solutions of the basic equations. Even if they are stable their basins of attraction decrease with increasing

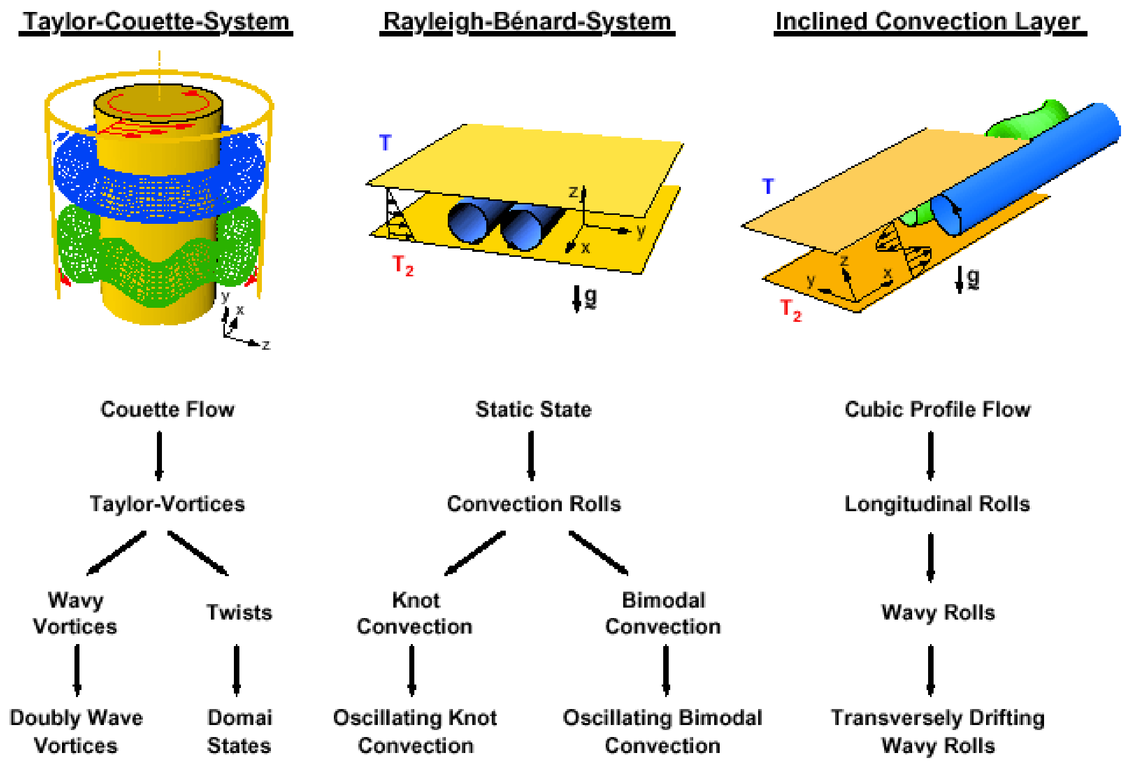

Figure 1: Examples of fluid systems with maximal symmetries and the typical sequence of bifurcations observed, starting with the basic roll solution.

control parameter and solutions describing more irregular spatio-temporal flow structures are typically observed in experimental realizations. Nevertheless, the regular, spatially periodic solutions usually exhibit most clearly the dynamical properties and transport mechanisms of the fluid system as a function of the control parameter.

2 Secondary Solutions

We now consider bifurcations which occur far from the critical point at which the laminar flow state becomes linearly unstable to roll patterns. We have seen in the previous lecture that the minimizing wave-vector of the most critical disturbance is infinitely degenerate when there is isotropy in the xy-plane. Here a weakly non-linear analysis is not suitable to detect bifurcations from secondary roll solutions because the non-linear terms in the Navier-Stokes equations play an equal role far from the linear stability point. Often isotropy manifests itself as phase turbulence for near critical parameter values, we therefore disregard isotropy so that we can analyze bifurcations from a roll solution with only one preferred direction. The basic equation can be written in the following canonical form

A	translation in time	$\partial\varphi/\partial t = 0$
B	translation along roll axis	$\partial\varphi/\partial x = 0$
C	transverse periodicity	$\varphi(y + 2\pi/\alpha, z) = \varphi(y, z)$
D	transverse reflection	$\varphi(-y, z) = \varphi(y, z)$ or $a_{-mn} = a_{mn}$
E	inversion about roll axis	$\varphi(\pi/\alpha - y, -z) = -\varphi(y, z)$ or $a_{mn} = 0$ for $m + n =$ odd

Table 1: Symmetry properties of two-dimensional rolls

$$\mathbf{L}\varphi - R\,\mathbf{B}\varphi - \mathbf{V}\frac{\partial}{\partial t}\varphi = \mathbf{N}\varphi\varphi \tag{1}$$

where $\mathbf{L}$, $\mathbf{B}$ and $\mathbf{V}$ are linear functionals and $\mathbf{N}$ represents the non-linear terms of the governing equations. The control parameter is now called R and homogeneity in two spatial dimensions and in time is assumed, therefore the functionals above may only depend on z.

The stability of the basic state with respect to infinitesimal disturbances φ_0 is governed by equation (1) with vanishing right hand side. Without loss of generality a disturbance of the form

$$\varphi_0 \propto exp\{i\mathbf{q}\cdot\mathbf{x} + \sigma t\} \tag{2}$$

can be assumed, where $\mathbf{x}$ is the position vector and where the wave-vector $\mathbf{q}$ lies in the x, y-plane. The critical point R_c is defined to be the point at which the real part σ_r of the growth rate of the most unstable solution vanishes. In the case of no isotropy typically the minimizing solution is unique and the imaginary part σ_i of the growth rate vanishes. Taking the y direction to be parallel to the minimizing wave-vector $\mathbf{q}_c$ and $\alpha \equiv\mid \mathbf{q}_c \mid$ we can write the two dimensional solution bifurcating from the basic state as a Galerkin expansion

$$\varphi = \sum_{m,n>0} a_{mn} \exp\{im\alpha y\} f_n(z) \tag{3}$$

where $f_n(z) = (-1)^{n-1} f_n(-z)$ for symmetry about midplane.

In table 1 we list the symmetry properties of rolls. They can be divided into the first three which are obeyed by all solutions of the form (3) and the remaining fourth and fifth which are satisfied in special cases. The fifth symmetry can occur only in problems such as Boussinesq Rayleigh-Bénard convection which have midplane symmetry.

The stability of secondary solutions can be studied through the superposition of infinitesimal disturbances of the form

$$\tilde{\varphi} = \exp\{ibx + idy + \sigma t\} \sum_{m,n>0} \tilde{a}_{mn} \exp\{im\alpha y\} f_n(z). \tag{4}$$

When equation (1) is linearized in the disturbance $\tilde{\varphi}$ an homogeneous linear equation for the unknowns $\tilde{a}_{mn}$ is obtained with the growth rate σ as eigenvalue. This linear eigenvalue problem for σ is just

$$\mathbf{L}\tilde{\varphi} - R\,\mathbf{B}\tilde{\varphi} - \mathbf{V}\sigma\tilde{\varphi} = \mathbf{N}\tilde{\varphi}\varphi + \mathbf{N}\varphi\tilde{\varphi} \tag{5}$$

Properties of disturbances		$\sigma_i \neq 0$	$b \neq 0$	$d \neq 0$	$\tilde{a}_{mn} \neq \tilde{a}_{-mn}$	$\tilde{a}_{mn} \neq 0$ for $m+n =$ odd
Symmetries Broken		translation in time	longitudinal translation	transverse periodicity	transverse reflection	inversion about axis
Eckhaus				X	X	
Crossroll	CR		X			X
Knot	KN		X			X
Even Blob	EB	X	X			
Odd Blob	OB	X	X			X
Oscillatory	OS	X	X		X	
Zig-Zag	ZZ		X		X	
Skewed Varicose	SV		X	X	X	
Osc. Skewed Var.		X	X	X	X	

Table 2: Symmetries Broken by Bifurcations from Steady Rolls

Of primary interest here are the growth rates σ with largest real part σ_r as a function of the horizontal wavenumbers b and d. The growing disturbances correspond to a transition of the roll solution to tertiary solutions which exhibit more shapes and styles and which reflect the specific physical conditions to a higher degree. Table 2 characterizes each type of instability that can occur from steady rolls. The skewed varicose instability leads most quickly to turbulent convection. Each of these instabilities can be observed for some values of $Pr - \alpha$. Figure 2 shows the enclosed domain of $Ra - \alpha - Pr$ space where roll solutions are stable. The Eckhaus instability usually causes rolls in an unstable region to be replaced by rolls in the stable region. Therefore the Eckhaus instability corresponds to a limitation of the available wavenumber for rolls and does not lead to a new type of solution.

3 Tertiary Solutions

Tertiary solution are twice spatially periodic solutions bifurcating from roll patterns. They can be described by expressions of the form

$$\varphi = \sum_{l,m,n} a_{lmn} \exp\{il\alpha_x x + im\alpha_y y\} f_n(z) \tag{6}$$

where we must have $a_{-l-mn} = a^+_{lmn}$ for a real solution, where $(\quad)^+$ denotes complex conjugation. We have assumed that the instability of interest has $\sigma_i = 0$. When an instability with a finite value of $\sigma_i = 0$ occurs, it typically leads to traveling waves propagating in the x direction which can be described by the representation above if x is replaced by $\hat{x} = x - ct$. A partial list of tertiary solutions is given in Table 3.

The stability of these steady three-dimensional solutions can then be studied through the superposition of infinitesimal disturbances of the form

$$\tilde{\varphi} = \exp\{ibx + idy + \sigma t\} \sum_{l,m,n} \tilde{a}_{lmn} \exp\{il\alpha_x x + im\alpha_y y\} f_n(z), \tag{7}$$

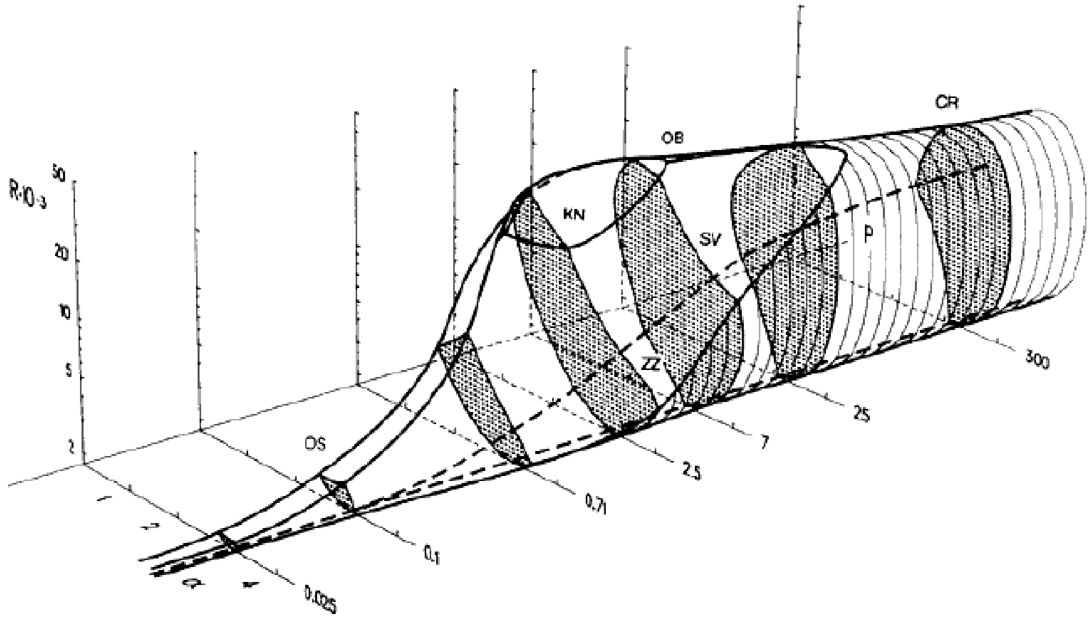

Figure 2: Region of stable convection rolls in the $Ra - \alpha - Pr$ parameter space. The region of stable rolls is bounded by surfaces corresponding to the onset of instabilities listed in Table 2. Note that Pr corresponds to P in the figure and increases toward the right and R corresponds to Ra.

Tertiary Solution	Reflection Symmetries	Inversion Symmetry
knot-/bimodal convection	$a_{-lmn} = a_{lmn} = a_{l-mn}$	$a_{lmn} = 0$ for $l + m + n =$ odd
undulating rolls	$a_{-lmn} = a_{lmn}$, $a_{l-mn} = (-1)^l a_{lmn}$	$a_{lmn} = 0$ for $m + n =$ odd
Symmetric traveling wave convection or wavy rolls with Poiseuille flow	$a_{l-mn} = (-1)^l a_{lmn}$	$a_{lmn} = 0$ for $m + n =$ odd
Wavy rolls with Couette flow or wavy Taylor vortices in small gap limit	$a_{l-mn} = (-1)^l a_{lmn}$	$a_{lmn} = (-1)^{m+n} a_{-lmn}$
Traveling blob convection	$a_{-lmn} = a_{lmn}$	$a_{lmn} = 0$ for $l + m + n =$ odd

Table 3: Examples of tertiary solutions and their symmetries listed in terms of the complex coefficients

where the coefficients $\tilde{a}_{lmn}$ can be found by substituting φ into equation (1), projecting onto the expansion functions, and solving the resulting non-linear equations using a Newton type method for some suitable spatial truncation size. The transition from tertiary to quarternary solutions is associated with the solution becoming time dependent. A much richer class of dynamical mechanisms for heat transport then become possible.

4 Quarternary Solutions

After the onset of three-dimensional tertiary solutions the continuous spatial symmetries such as the invariance with respect to the translation along the roll axis have been broken and have been replaced by reflection symmetries and inversion symmetries such as those shown in Table 3. The stability of the steady or traveling tertiary solutions can be investigated through the superposition of arbitrary infinitesimal disturbances. Using the general Floquet ansatz

$$\tilde{\varphi} = \exp\{ibx + idy + \sigma t\} \sum_{l,m,n} \tilde{a}_{lmn} \exp\{il\alpha_x x + im\alpha_y y\} f_n(z) \tag{8}$$

we arrive at a linear homogeneous system of equations for the unknown coefficients $\tilde{a}_{lmn}$ with the growth rate σ as eigenvalue. When the maximum real part of σ as a function of d and b is less or equal to zero the tertiary solution is stable. Otherwise it is unstable.

The most strongly growing disturbances of tertiary stationary solutions are often those with non-vanishing imaginary part of σ_i. Since traveling wave type solutions are no longer possible after the translational invariance along the axis of the rolls has been broken, the time dependence must be taken into account explicitly. Time dependent three-dimensional solutions can be obtained through forward integration in time of the differential equations for the time dependent coefficients $a_{lmn}(t)$ in the representation for the quarternary solutions.

$$\varphi = \sum_{l,m,n} a_{lmn}(t) exp\{il\alpha_x x + im\alpha_y y\} f_n(z) \tag{9}$$

The system of differential equations is obtained, just as in the case of the algebraic equations of tertiary solutions through projections of the equations of motion onto the space of the expansion functions. Examples of quarternary solutions, that is solutions in three-dimensions and the fourth dimension time, include oscillatory bimodal convection, oscillatory knot convection and pulsating traveling blob convection.

5 Bimodal Convection

5.1 Steady Bimodal Convection: An example of a tertiary solution

Steady bimodal convection is an example of a tertiary solution in Rayleigh-Bénard convection (see Figure 1). It corresponds to the superposition of a secondary roll pattern with smaller wavelength onto the given roll pattern as shown in the sketch in Figure 3. Through

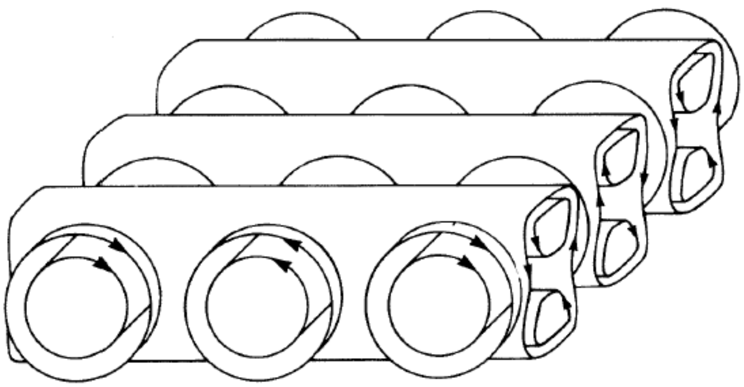

Figure 3: Schematic sketch of bimodal convection in a fluid heated from below. Note the superposition of a secondary roll pattern on the already existing roll pattern.

the onset of bimodal convection the convective heat transport becomes more efficient and the two roll patterns quickly reach comparable amplitudes as the Rayleigh number is increased beyond onset.

5.2 Transition to Bimodal Convection: An heuristic argument

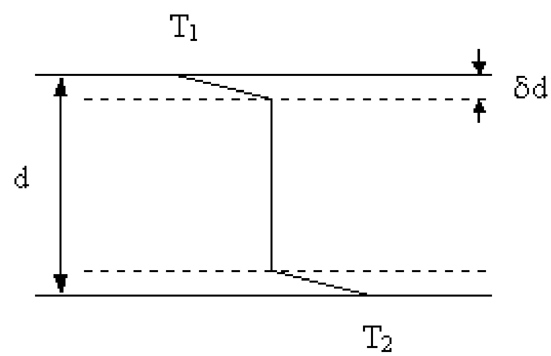

Figure 4: The approximate form of the temperature profile for steady roll patterns

In Rayleigh-Bénard convection the mean temperature field for steady roll solutions has vanishing gradient in the interior of the flow and strong gradients near to the boundary. We can think of this thermal boundary layer as a subconvection layer with rescaled Rayleigh number $\frac{R}{2}\delta^3$, where δ is the non-dimensional thickness of the boundary layer. This situation is illustrated in Figure 4. The condition for convective instability in this layer is the Rayleigh condition for instability $\frac{R}{2}\delta^3 > R_c$. If we assume that the gradient of temperature in the subconvection layer is approximately constant then the heat transport is $H \approx \frac{R}{2\delta}$ and we can write the condition for instability of the boundary layer as

$$H < \frac{R}{2}\left(\frac{R}{2R_c}\right)^{1/3}.$$

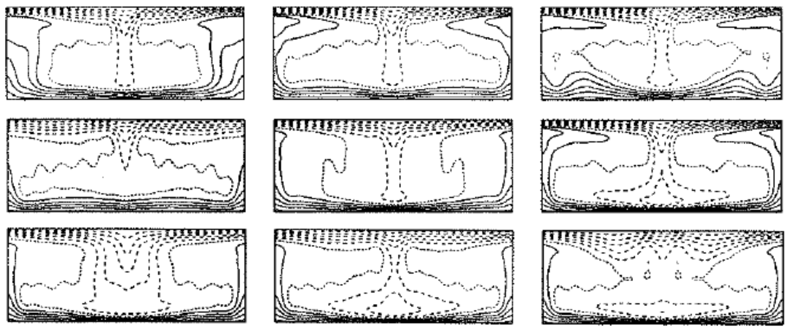

Figure 5: Isotherms at the y, z-planes $x = 0, x = \pi/\alpha_x$ (from top to bottom) at the times $t = n\pi/3\omega$ for $n = 0, 1, 2$. y increases toward the right and z increases upward. The parameter values $Pr = 30, Ra = 10^5, \alpha_x = 4.5, \alpha_y = 2.5$ have been used.

The most efficient configuration for heat transport to result from this type of instability is for tight boundary layer convection rolls to align perpendicular to the primary convection rolls as exemplified in the bimodal solution.

5.3 Oscillatory Bimodal Convection: An example of a quarternary solution

An example of these types of convection patterns in nature could be the formation of bimodal convection patterns in clouds, which exhibit a very distinct rectangular pattern in the sky. They are typically high in Prandtl number and have a scale of the order of 100m across. If the Prandtl number is in the range $10 \lesssim Pr \lesssim 10^2$ the bifurcation from rolls to bimodal cells is followed by a further bifurcation to oscillatory bimodal convection. The thermal boundary layers periodically thicken and blobs of fluid hotter or cooler than average circulate through the convection cells. These oscillations are characterized to some extent by a resonance between the circulation time of the bimodal cell and the period of thickening and thinning of the thermal boundary layers.

There are two types of oscillatory bimodal convection, the symmetric one that does not change the spatial symmetry of steady bimodal convection and the other, called wavy oscillatory bimodal convection, which is characterized by the property that the set of coefficients $a_{lmn}(t)$ with

$$-a_{-lmn} = a_{lmn} = a_{l-mn} \text{ for } l + m + n = \text{odd} \text{ and } a_{lmn} = 0 \text{ otherwise} \tag{10}$$

are participating in the description of the solution in addition to those listed in Table 3 for bimodal convection. Figure 5 provides an impression of the time dependent structure of wavy oscillatory bimodal convection taken from numerical computations of [1] and in Figure 6 an experimental visualization is depicted. In the first we see a blob of cold fluid descending and impinging on the bottom of the layer while in the second figure we distinctly see the walls of the bimodal cells flexing back and forward.

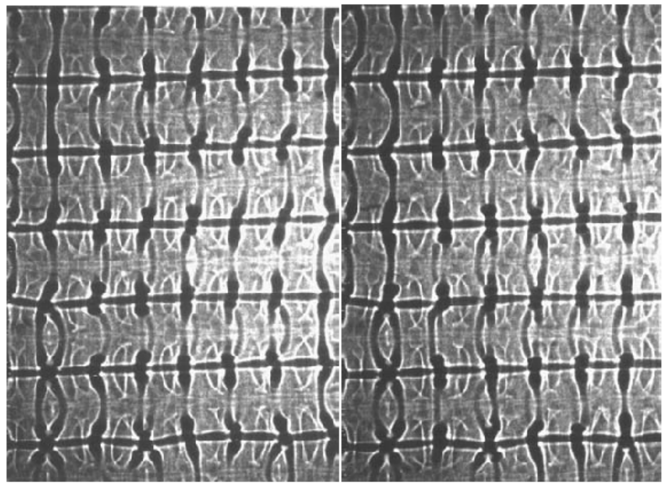

Figure 6: Shadowgraph observation of wavy oscillatory bimodal convection in a layer of silicon oil heated from below. The dark regions indicate hot rising fluid. The Prandtl and Rayleigh numbers are $Pr = 63$, $Ra = 1.5 \times 10^5$ and the wave numbers in the x-direction (toward the right) and y-direction are given by $\alpha_x = 4.08$, $\alpha_y = 2.04$. The right photograph was taken 25 seconds after the left one which corresponds to nearly half a period. Along the darker vertical lines small arches may be observed, pointing to the right or left, these are due to the oscillatory behaviour of the system.

It should be kept in mind that the realization of convection flows that are periodic in space and in time requires controlled initial conditions such that an approximately perfect roll pattern is realized after the onset of convection. The transition to bimodal attractors is sufficiently strong such that pattern imperfections can be eliminated in time except close to the sidewalls. The transition to oscillations usually occurs in a less homogeneous way and their phases tend to exhibit large scale variations. Without controlled initial conditions the convection flows at onset occur already in the form of patches of rolls with different horizontal orientations which tend to evolve in such a way that they ultimately reflect the geometrical configuration at the sidewalls of the layer, see the right column of shadowgraphs in Figure 8. As the Rayleigh number increases, the density of dislocations in the pattern increases rapidly and a chaotic structure of a kind of bimodal convection is realized when the Prandtl number is sufficiently high ($Pr \gtrsim 10$). The onset of oscillations in the form of hot and cold blobs emerging from the thermal boundary layer occurs initially at a few spots where the convection pattern deviates most strongly from the ideal periodic form. Laboratory experiments thus exhibit in general a more turbulent situation in qualitatively the same manner as in the case of the spatially and temporarily periodic solutions produced by the sequence of bifurcation approach. The latter method thus provides a sensible way toward an understanding of the processes occurring in turbulent convection as well as in other cases of fluid turbulence.

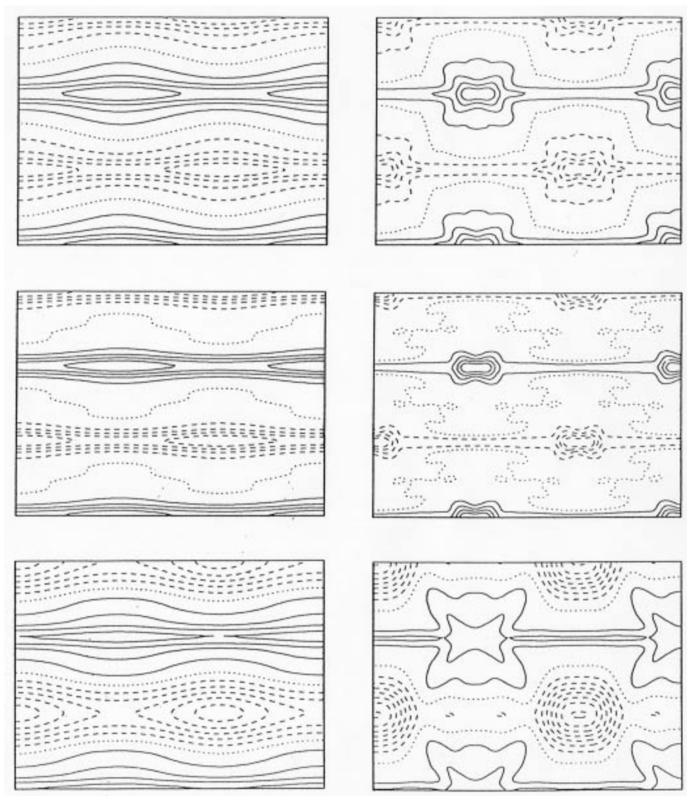

Figure 7: Numerical results for simulations of steady knot convection.The views are planar. The top two graphs show an average of the heat flux over the entire depth, z of the convective layer, the two graphs in the middle show a section through the centre of the layer, $z = 0$ and the bottom two graphs show a flux of the heat through the bottom boundary. Left hand column: $R = 2.5 \cdot 10^4$, right hand column $R = 8 \cdot 10^4$.

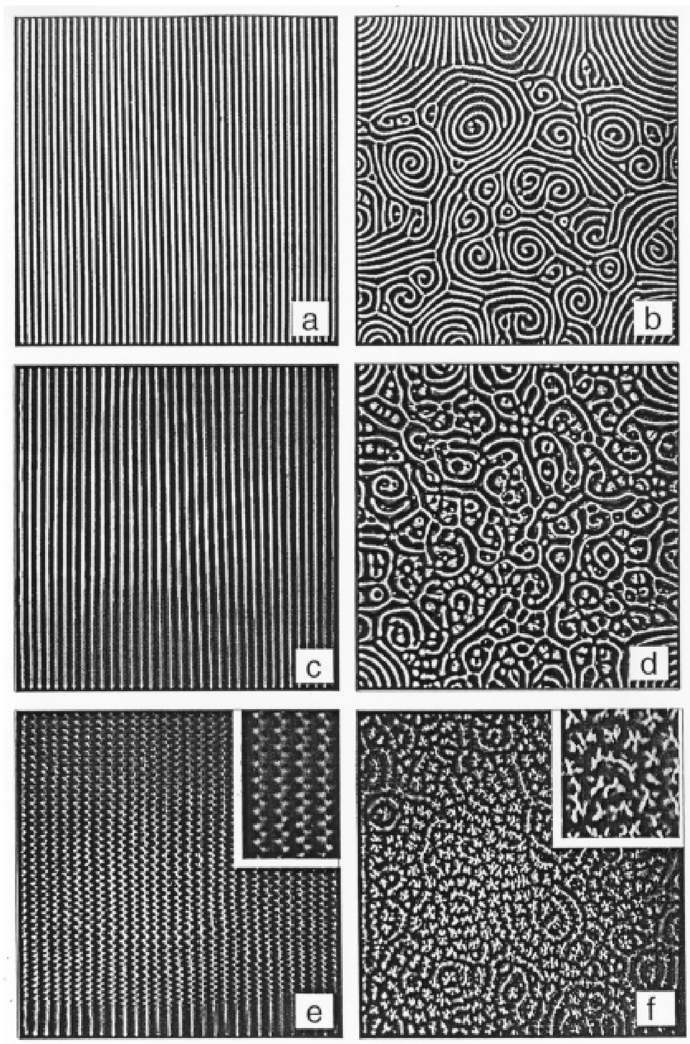

Figure 8: Digitally enhanced shadowgraph images of the convection patterns (taken from [2]). The distance from the critical point for onset of convection is measured as $\epsilon = (R - R_c)/R_c$: (a) and (b) $\epsilon = 0.920$; (c) $\epsilon = 2.986$, (d) $\epsilon = 3.000$, (e) and (f) $\epsilon = 5.082$. The left column shows the effect of increasing the Rayleigh number on a field of rolls with uniform orientation, while the initial state in the right column contains patches of rolls oriented in arbitrary directions. As the Rayleigh number is increased the rolls undergo transition to wavy rolls.

References

[1] R. Clever and F. Busse, "Steady and Oscillatory Bimodal Convection," J. Fluid Mech. **271**, 103 (1994).

[2] R. Cakmur, D. Egolf, B. Plapp, and E. Bodenschatz, "Bistability and competition of spatiotemporal chaotic and fixed point attractors in Rayleigh-Benard convection," Phys. Rev. Lett. **79**, 1853 (1997).